

# Symmetry protection of topological states in multimode photonic resonator chains

A. Tikan,<sup>1,\*</sup> A. Tusnin,<sup>1</sup> J. Riemensberger,<sup>1</sup> M. Churaev,<sup>1</sup>  
K. Komagata,<sup>1,2</sup> X. Ji,<sup>1</sup> R. N. Wang,<sup>1</sup> J. Liu,<sup>1</sup> and T. J. Kippenberg<sup>1,†</sup>

<sup>1</sup>*Institute of Physics, Swiss Federal Institute of Technology Lausanne (EPFL), CH-1015 Lausanne, Switzerland*

<sup>2</sup>*Present address: Laboratoire Temps-Fréquence, Avenue de Bellevaux 51, 2000 Neuchâtel, Switzerland*

(Dated: December 22, 2024)

The driven dissipative nonlinear multimode photonic dimer is considered as the simplest case of solitons in photonic lattices. It supports a variety of emergent nonlinear phenomena including gear soliton generation, symmetry breaking and soliton hopping. Surprisingly, it has been discovered that the accessibility of solitons in dimers drastically varies for the symmetric and anti-symmetric supermode families. Linear measurements reveal that the coupling between transverse modes, that give rise to avoided mode crossings, can be almost completely suppressed. We explain the origin of this phenomenon which we refer to as symmetry protection. We show its crucial influence on the dissipative Kerr soliton formation process in lattices of coupled high Q resonators of any type. Examining topologically protected states in the Su-Schrieffer-Heeger model of coupled resonators, we demonstrate that topological protection is not sufficient against the transversal mode crossing induced disorder. Finally, we show that the topological edge state can be symmetry protected by carefully choosing the balance between intra- and inter-resonator coupling to higher-order transverse modes, which suppresses mode crossings.

Avoided crossings of molecular potential energy surfaces for states with the same point group symmetry (see Fig. 1a), as first pointed out by von Neumann and Wigner [1] in the early years of molecular quantum mechanics, are today standard textbook knowledge [2]. Longuet-Higgins using a topological reasoning, which anticipated the notion of Berry phase [3, 4], has shown that energy surface *crossings* - rather than avoided crossings as in diatomic molecules - can arise in polyatomic arrangements [5]. Rising doubts about the overall validity of the approach in a series of papers [6, 7] (which has been a subject of substantial criticism, see for example [8]), Hatton and co-authors pointed out the presence of *conical crossings* in single-electron diatomic ions and highlighting the role of off-diagonal terms in the Hamiltonian matrix. Later, by means of computer simulations it was shown that conical crossings are a rather common phenomenon and are critical in many molecular reaction and relaxation processes [9].

The analogy between molecules and coupled resonators systems has been discussed in various studies [10–12]. Similar to the molecular energy surfaces, different eigenmode families of an optical resonator experience avoided mode crossings (AMXs) which leads to distortions of initially smooth (i.e. unperturbed) dispersion profile [13–16] as shown in Fig. 1a,b. These dispersion profiles are important in a plethora of resonant nonlinear wave-mixing schemes and especially in the context of dissipative Kerr soliton (DKS) generation in resonators possessing  $\chi^{(3)}$  nonlinear susceptibility [17]. DKSs are localized stable structures found in driven dissipative nonlinear resonators [18, 19]. The shape of DKS is given by the balance between dispersion and Kerr nonlinearity which results (in the simplest case) in the characteristic hyperbolic secant profile on a continuous wave background,

while its amplitude is fixed due to the balance between coupling losses and parametric gain [20–22]. The generation of DKS in passive microresonators [19] that can be integrated on chip [23], has triggered the development of compact broadband high-repetition frequency combs for applications ranging from dual-comb spectroscopy [24], multichannel optical communication [25], and distance metrology [26–28]. Even though AMXs have been successfully employed to trigger the nonlinear dynamics in normal dispersion resonators [29–32] and to control disorder in perfect bright soliton crystals [33], it remains an undesirable effect as it disrupts the DKS formation process [16] and can induce instabilities such as intermode breathing [34].

Recently, the possibility of DKS generation in a photonic dimer (i.e. strongly coupled optical resonators) has been investigated both experimentally and numerically [35]. DKSs can be generated in one of the hybridized dimer supermodes which are called, in analogy with molecular systems, symmetric (S) and antisymmetric (AS) as depicted in Fig. 1b. Hybridized supermodes are split by  $\Delta\omega = \sqrt{4(J_{aa}^{\text{ext}})^2 + \delta^2}$ , where  $J_{aa}^{\text{ext}}$  is the coupling between fundamental modes of the resonators and  $\delta$  is inter-resonator detuning. Integrated dispersion is defined as  $D_{\text{int}}(\mu) = \omega_\mu - (\omega_0 + D_1\mu)$ , where  $\mu$  is the mode index and  $D_1/2\pi$  corresponds to the free spectral range at frequency  $\omega_0$ . Due to the underlying symmetry, DKSs generated in the photonic dimer supermodes are termed as "gear solitons". Also, this study revealed a variety of emergent nonlinear phenomena including periodic appearance of commensurate and incommensurate dispersive waves, symmetry breaking related to the discreteness of the dispersion profile, and soliton hopping which requires the DKSs generation in both supermodes. Recent works on different implementations of coupled res-

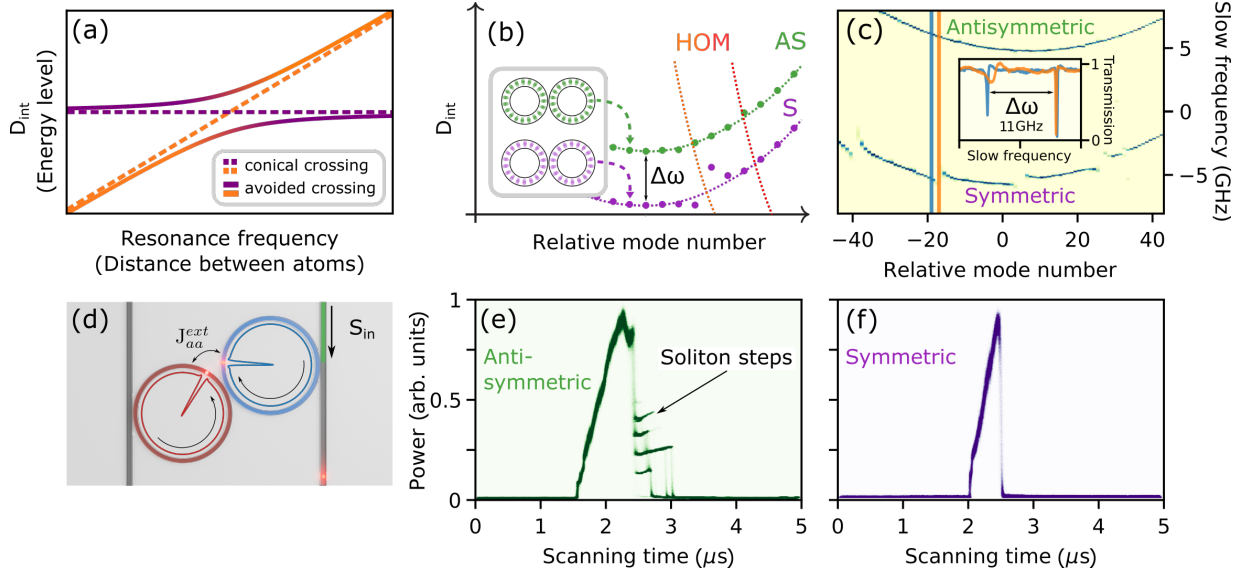


FIG. 1. **Effect of symmetry protection in the photonic dimer and gear soliton generation.** (a) Avoided and conical crossings in resonators and molecular systems.  $D_{\text{int}}$  stands for integrated dispersion. (b) Schematic dispersion profile of the photonic dimer showing anomalous modal crossing. HOM stands for higher-order modes, AS - for antisymmetric mode, and S - for the symmetric modes. Inset shows the corresponding hybridized field distribution. (c) Dispersion profile measurements of the photonic dimer. Inset shows two cross-sections of plot (c) at mode numbers -19 and -17. (d) Schematic representation of the photonic dimer and gear solitons generation. (e,f) Experimental recording of generated light in AS and S modes of the photonic dimer, respectively. Each plot contains 600 superimposed oscilloscope traces.

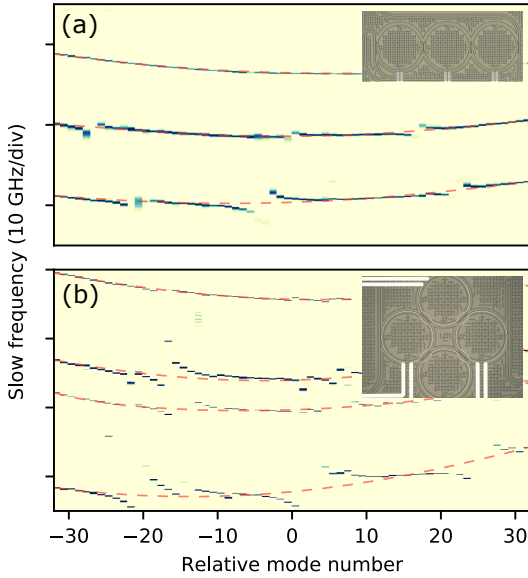


FIG. 2. **Linear dispersion measurements of nontrivial resonator arrangements.** (a) Chain of three resonators. (b) Square lattice. Dashed lines show expected mode profiles without the influence of avoided mode crossings.

onator pairs promise great application potential due to demonstrated enhancement of the soliton generation efficiency [36] and possibility to obtain a flat and broadband solitonic spectrum [35].

Some of the numerically predicted effects (such as soli-

ton hopping) were not observed in the experiment, and an unexpected phenomenon obstructing their observation has been discovered. Namely, the linear transmission spectroscopy of the photonic dimer revealed that the AS supermode family is *protected against the AMXs* while the S supermode family interacts with higher-order modes stronger than expected (see Fig. 1b,c and Sup. Mat. in [35]). The presence of AMX in the S supermode family strongly disrupts DKS generation and completely suppresses the DKS formation at moderate power levels. The effect of vanishing interaction between transversal mode families, which we call *symmetry protection*, exhibits remarkable similarities with the anomalous potential energy surfaces crossings in diatomic ions [6]. It is expected to be universal and ubiquitous in strongly coupled resonator chains and lattices enabling robust access to gear solitons in the protected supermodes. Symmetry protection is expected to play a crucial role in the emerging field of soliton lattices (i.e. lattices of driven nonlinear resonators exhibiting global and local mode-locking).

Experimental evidences of the symmetry protection effect are obtained with strongly coupled microrings having 200 GHz free spectral range and loaded Q-factor of the order of 2 millions, realized on  $\text{Si}_3\text{N}_4$  platform using the photonic Damascene reflow process [37]. The intrinsic loss rate of the dimer is 50 MHz, and both resonators are interfaced with bus waveguides with external coupling rates of 100 MHz. Employing frequency comb calibrated diode laser spectroscopy - a well-established technique

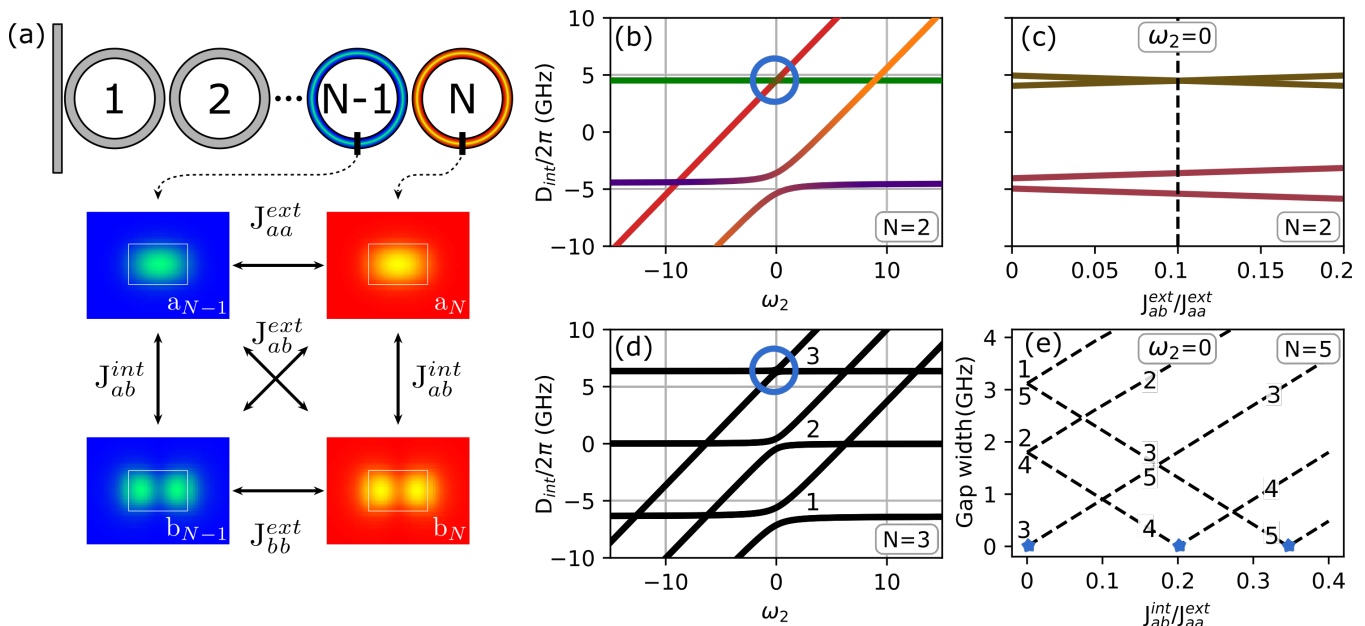


FIG. 3. **Symmetry protection in coupled resonators.** (a) Schematic representation of coupled resonators chain and description of the coefficients of the coupling matrix used in Eq. 2. (b) Symmetry protection in the photonic dimer. Protected state is highlighted by the blue circle. Green line corresponds to AS fundamental mode, violet to S fundamental mode, red - AS higher-order mode, and orange - S higher-order mode. Parameters are chosen to be close to the experimental ones:  $J_{aa}^{\text{ext}}/2\pi = 4.5$  GHz,  $J_{ab}^{\text{int}} = J_{ab}^{\text{ext}} = 0.1J_{aa}^{\text{ext}}$  (c) The splitting between hybridized supermodes with coinciding central frequencies. Dashed black line shows the parameters corresponding to plot (b). (d) Symmetry protection in the trimer configuration. (e) The gap distance between split resonances as a function of  $J_{ab}^{\text{int}}/J_{aa}^{\text{ext}}$  for a chain of 5 coupled resonators. Lines are numbered according to the symmetry of the modes as shown in plot (d). Blue stars depict the symmetry protected states.

which has been used in a variety of studies (see for example [38]) - we retrieve first the dispersion profile of the photonic dimer (Fig. 1c). It is represented in terms of slow frequency which has been defined as  $D_{\text{int}}/2\pi$  with an arbitrary shift. The profile reveals two dimer supermode families. The interaction with higher-order modes drastically differs for the two supermodes. The fundamental S supermode family is strongly affected by AMXs leading to the periodic discontinuity of the dispersion profile while the AS mode dispersion profile is almost unperturbed. We systematically study the influence of AMXs on the generation of gear solitons. Fig. 1e,f shows a superposition of 600 transmission traces obtained by sweeping the pump laser frequency over the AS and S resonances at 1554 nm with an optical power in the waveguide of 43 mW [19]. We use a conventional CW pumping scheme combined with fast single side-band tuning to eliminate thermal heating and resonance shifts [39]. Transmission profiles for the AS mode show the presence of characteristic steps signifying stable access to the solitonic state [40]. Contrary, S mode profiles do not exhibit any solitonic feature at the equivalent pump power. At significantly lower input power, soliton generation can also be observed in the symmetric mode family (see Supplementary Materials), highlighting the disruptive effect of the AMX.

As pointed out in [41] presence of the AMX leads to intense generation of dispersive waves which perturb the solitonic state. Each soliton acts as a source of dispersive waves and, therefore, the number of solitons is naturally reduced until the perturbation becomes sufficiently weak to maintain the state. The strength of the perturbation depends on the position of AMX since the power spectral density envelope of the solitonic state and, hence, the energy transferred to the higher-order mode, decays exponentially from the pumped mode.

A similar effect is observed for the trimer configuration (i.e. chain of three strongly coupled resonators). Linear dispersion measurements (see Fig. 2a) reveal that the symmetry protection effect is the strongest for the most antisymmetric trimer supermode and decreases with increasing symmetry. We also investigate a more complex resonator arrangement representing a fundamental element of the square lattice. Fig. 2b shows the dispersion profile of a plaquette of resonators. In the ideal case two central mode families are degenerate but due to the presence of the finite inter-resonator detuning  $\delta$ , the degeneracy is lifted and we observe all four mode families. As follows from the plot, the effect of symmetry protection takes place even in this two-dimensional resonator system leading to a high distortion of the symmetric resonances.

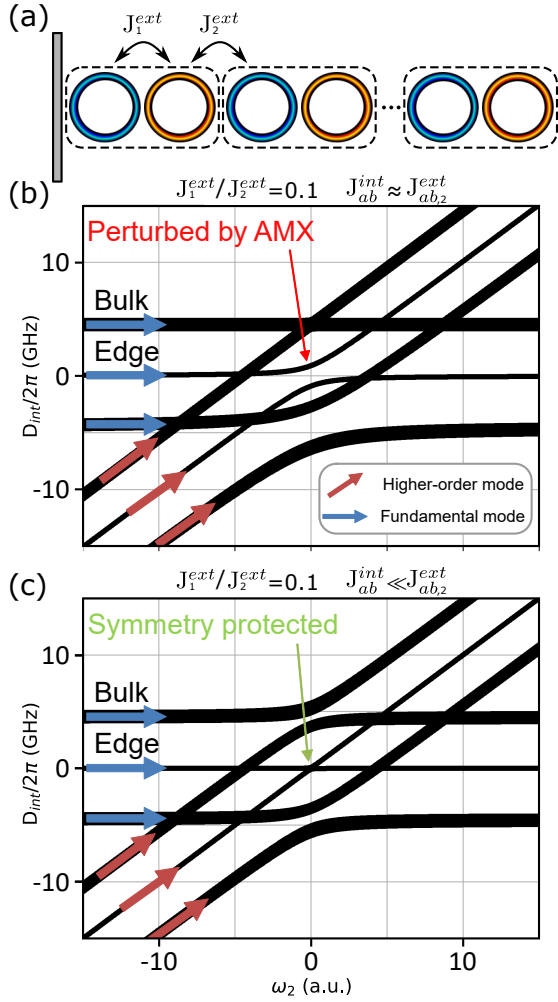


FIG. 4. **Symmetry protection against mode crossing of the topological edge state in Su-Schrieffer-Heeger model.** (a) Schematic representation of 10 coupled resonators with alternating coupling which constitutes the SSH chain. (b) Influence of AMX when  $J_{ab}^{\text{int}} \approx J_{ab,2}^{\text{ext}}$ . (c) The same configuration with  $J_{ab}^{\text{int}} \ll J_{ab,2}^{\text{ext}}$  exhibits the protection against AMX.

In order to shed light on the symmetry protection phenomenon, we derive from Maxwell's equations a Hermitian model of four coupled mode interaction (see Supplementary Materials). We consider two fundamental  $a_{1(2)}$  and two transverse higher-order  $b_{1(2)}$  modes of both resonators constituting the dimer. The coupled mode equations can be written as follows [42]:

$$i \frac{dU}{dt} = - \begin{pmatrix} -\omega_1 & J_{aa}^{\text{ext}} & J_{ab}^{\text{int}} & J_{ab}^{\text{ext}} \\ J_{aa}^{\text{ext}} & -\omega_1 & J_{ab}^{\text{ext}} & J_{ab}^{\text{int}} \\ J_{ba}^{\text{int}} & J_{ba}^{\text{ext}} & -\omega_2 & J_{bb}^{\text{ext}} \\ J_{ba}^{\text{ext}} & J_{ba}^{\text{int}} & J_{bb}^{\text{ext}} & -\omega_2 \end{pmatrix} U, \quad (1)$$

where  $U = (a_1, a_2, b_1, b_2)^\top$ . Eigenvalues of the coupling matrix can be found analytically. Assuming that the cou-

pling matrix is symmetric, we obtain:

$$\begin{aligned} \lambda_{1,2}(\text{as}) &= \\ \frac{1}{2} \left( 2J_{aa}^{\text{ext}} \pm \sqrt{4(J_{ab}^{\text{int}} - J_{ab}^{\text{ext}})^2 + (\omega_1 - \omega_2)^2} + \omega_1 + \omega_2 \right) \\ \lambda_{3,4}(\text{s}) &= \\ \frac{1}{2} \left( -2J_{aa}^{\text{ext}} \pm \sqrt{4(J_{ab}^{\text{int}} + J_{ab}^{\text{ext}})^2 + (\omega_1 - \omega_2)^2} + \omega_1 + \omega_2 \right). \end{aligned} \quad (2)$$

The notation for coupling coefficients is described in Fig. 3a.  $J_{aa}^{\text{ext}}$  corresponds to the coupling between fundamental modes of the nearest resonators,  $J_{ab}^{\text{ext}}$  - to the coupling between fundamental mode of one resonator and higher-order mode of the neighbour, and  $J_{ab}^{\text{int}}$  is the coupling between fundamental and higher-order mode within the same resonator. The coupling strength between two higher-order modes is set to  $J_{aa}^{\text{ext}}$  since it does not qualitatively change the result. The difference between  $J_{aa}^{\text{ext}}$  and  $J_{bb}^{\text{ext}}$  will lead to a shift of the hybridization area along the direction of the higher-order mode. As an example of the higher-order resonator mode we show  $\text{TE}_{10}$ .

Thus, we find two pairs of eigenvalues that represent the mode interaction. The first couple  $\lambda_{1,2}$  corresponds to the AS supermodes while  $\lambda_{3,4}$  to S one. The expression under the square root in the first couple of eigenvalues contains the term  $(J_{ab}^{\text{int}} - J_{ab}^{\text{ext}})^2$ . Therefore, in the case when  $J_{ab}^{\text{int}}$  and  $J_{ab}^{\text{ext}}$  are of the same order the influence of the AMX is reduced. However, in the second couple eigenvalues the effect of AMX is increased in comparison to the conventional hybridization in the single resonator case.

Indeed, numerical simulations of the coupling region for parameters close to experimental ones (see Supplementary Materials) demonstrated that the ratio between  $J_{ab}^{\text{ext}}$  and  $J_{ab}^{\text{int}}$  tends to one. The coupling sections to bus and drop waveguides will contribute to the coefficient  $J_{ab}^{\text{int}}$  as well, however, this contribution is found to be one order of magnitude smaller which is consistent with the experimentally observed strong symmetry protection of AS supermode parabola (Fig. 1c).

The eigenvalue system Eq. 2 as a function of the central frequency of the higher-order mode  $\omega_2$  with the ratio  $J_{ab}^{\text{int}}/J_{ab}^{\text{ext}} = 1$  is depicted in Fig. 3b. Fig. 3c shows the dependence of the positions of resonance for the hybridized modes in the case when  $\omega_1 = \omega_2$  (at the center of Fig. 3b) as a function of  $J_{ab}^{\text{ext}}/J_{aa}^{\text{ext}}$ . Black dashed line corresponds to the conditions considered in Fig. 3b. As predicted from Eq. 2, when  $J_{ab}^{\text{int}}$  and  $J_{ab}^{\text{ext}}$  coincide exactly, the gap distance tends to zero. The structure of the coupling matrix in Eq. 1 is remarkably similar to the Hamiltonian discussed in [6], which underpins the profound nature of the proposed analogy with molecular system.

This model can be easily extended to the case of arbitrary number of resonators (see Supplementary Materials). An example of the mode hybridization for the

trimer configurations is shown in Fig. 3d. Influence of the AMX increases with the increasing symmetry as suggested by the experimental data. Numerical analysis of larger chains revealed that the index of symmetry protected mode depends on the values  $J_{ab}^{\text{ext}}$  and  $J_{ab}^{\text{int}}$  and, therefore, *can be manipulated*. When the coupling between the fundamental mode of one resonator and the higher-order mode of its neighbour can be neglected then the effect of AMXs is the same for all the hybridized mode. In the opposite case, when the coupling between modes within one resonator is weak ( $J_{ab}^{\text{int}} \ll J_{ab}^{\text{ext}}$ ) the symmetry protection falls into the middle mode family and symmetrically decreases towards modes with higher and lower symmetries. Therefore, the symmetry protection can be moved along the dispersion relation by changing the coupling coefficients ratio. Fig. 3e shows the dependence of the AMX-induced gap width as a function of normalized  $J_{ab}^{\text{int}}$  coefficient for five resonators coupled in a chain. When the photon transfer to the higher-order mode of the neighbouring ring can be neglected, the middle mode (3) becomes symmetry protected. With increasing  $J_{ab}^{\text{int}}$  the symmetry protection moves towards the fourth mode family and subsequently to the fifth one, i.e. the most anti-symmetric.

In order to highlight the importance of symmetry protection for the future development of field of the soliton lattices, we study the effect of AMXs on topologically protected edge states in the Su–Schrieffer–Heeger (SSH) model [43] originally proposed for the explanation of mobile neutral defects in polyacetylene. Due to the simplicity of implementation [44], this model often serves as a primary verification platform for novel nonlinearity-related topological effects [45]. It can be easily implemented in our system by varying the inter-resonator coupling coefficients  $J_{aa}^{\text{ext}}$  and  $J_{ab}^{\text{ext}}$ . Schematic representation of the SSH model in coupled resonator is shown in Fig. 4a. The alternating coupling effectively divide the chain into a number of unit cells show by dashed rectangles. The coupling strength ratio inside a unit cell and between unit cells ( $J_1^{\text{ext}}/J_2^{\text{ext}}$ ) is chosen to be 0.1 which is sufficient for obtaining a nonzero winding number [46]. Fig. 4b shows the mode hybridization for the SSH model realized with ten resonators. The topologically protected (against the disorder and variation of the coupling coefficients) edge state is in the middle of the gap between two bulk states as noted in Fig. 4b. The same picture is observed in the higher-order mode family. According to the model, a crucial influence of AMX on the topological state is expected which potentially forbids or drastically obstructs the generation of topological gear solitons if the mode couplings and, therefore, the symmetry protection is not controlled. Increasing the difference between the  $J_{ab}^{\text{int}}$  and  $J_{ab,2}^{\text{ext}}$ , we observe enhancement of the symmetry protection effect on the edge state mode. This can be achieved by carefully designing the coupling section to suppress the internal transversal mode couplings.

Therefore, the proposed model suggests that the effect of symmetry protection is ubiquitous in multimode resonator chains. It must be always taken into account in order to stably excite gear soliton states or other nonlinear dynamical regimes that exist in photonic lattices. As almost all contemporary anomalous dispersion waveguide designs support multiple transversal modes, our results highlight the need to account for the increased excitation of higher-order modes in the coupling sections in order to scale DKS generation to multiple resonator structures and large (topological) photonic lattices.

In this article, we introduced the notion of symmetry protection in chains of coupled multimode resonators which exhibit a remarkable similarity with conical energy level crossings in molecular systems. The crucial influence of this effect on the dispersion profile and, therefore, the gear soliton generation is demonstrated experimentally. We propose a simple model which fully explains the effect. We discuss the possibility to manipulate the index of symmetry protected mode by changing the ratio between the coupling to the higher-order modes within the ring and between the neighbouring rings. We highlight the importance of this effect for the future development of the field by showing that topologically protected edge state in the SSH model can be highly influenced by AMXs and, therefore, it must be carefully taken into the account while designing the experimental platform for the observation of topological gear solitons.

## ACKNOWLEDGEMENTS

This publication was supported by Contract 18AC00032 (DRINQS) from the Defense Advanced Research Projects Agency (DARPA), Defense Sciences Office (DSO). This material is based upon work supported by the Air Force Office of Scientific Research, Air Force Materiel Command, USAF under Award No. FA9550-19-1-0250. This work was further supported by the European Union’s Horizon 2020 Program for Research and Innovation under grant no. 846737 (Marie Skłodowska-Curie IF CoSiLiS), 812818 (Marie Skłodowska-Curie ETN MICROCOMB), 722923 (Marie Skłodowska-Curie ETN OMT). Si<sub>3</sub>N<sub>4</sub> samples were fabricated and grown in the Center of MicroNanoTechnology (CMi) at EPFL.

---

\* [alexey.tikan@epfl.ch](mailto:alexey.tikan@epfl.ch)

† [tobias.kippenberg@epfl.ch](mailto:tobias.kippenberg@epfl.ch)

- [1] J. von Neumann and E. P. Wigner, in *The Collected Works of Eugene Paul Wigner* (Springer, 1993) pp. 294–297.
- [2] L. D. Landau and E. M. Lifshitz, *Quantum mechanics: non-relativistic theory*, Vol. 3 (Elsevier, 2013).

- [3] M. V. Berry, Proc. R. Soc. A **392**, 45 (1984).
- [4] T. Ozawa, H. M. Price, A. Amo, N. Goldman, M. Hafezi, L. Lu, M. C. Rechtsman, D. Schuster, J. Simon, O. Zeitlinger, and I. Carusotto, *Rev. Mod. Phys.* **91**, 15006 (2019), [arXiv:1802.04173](https://arxiv.org/abs/1802.04173).
- [5] H. C. Longuet-Higgins, *Proc. R. Soc. A* **344**, 147 (1975).
- [6] G. Hatton, W. Lichten, and N. Ostrove, *Chemical Physics Letters* **40**, 437 (1976).
- [7] G. J. Hatton, *Phys. Rev. A* **16**, 1347 (1977).
- [8] C. A. Mead, *J. Chem. Phys.* **70**, 2276 (1979).
- [9] D. R. Yarkony, *Rev. Mod. Phys.* **68**, 985 (1996).
- [10] M. Bayer, T. Gutbrod, J. Reithmaier, A. Forchel, T. Reinecke, P. Knipp, A. Dremin, and V. Kulakovskii, *Phys. Rev. Lett.* **81**, 2582 (1998).
- [11] S. V. Boriskina, “Photonic molecules and spectral engineering,” in *Photonic Microresonator Research and Applications*, edited by I. Chremmos, O. Schwelb, and N. Uzunoglu (Springer US, Boston, MA, 2010) pp. 393–421.
- [12] M. Zhang, C. Wang, Y. Hu, A. Shams-Ansari, T. Ren, S. Fan, and M. Lončar, *Nat. Photonics* **13**, 36 (2019).
- [13] T. Carmon, H. G. L. Schwefel, L. Yang, M. Oxborrow, A. D. Stone, and K. J. Vahala, *Phys. Rev. Lett.* **100**, 103905 (2008).
- [14] A. Savchenkov, A. Matsko, W. Liang, V. Ilchenko, D. Seidel, and L. Maleki, *Opt. Express* **20**, 27290 (2012).
- [15] Y. Liu, Y. Xuan, X. Xue, P.-H. Wang, S. Chen, A. J. Metcalf, J. Wang, D. E. Leaird, M. Qi, and A. M. Weiner, *Optica* **1**, 137 (2014).
- [16] T. Herr, V. Brasch, J. D. Jost, I. Mirgorodskiy, G. Lihachev, M. L. Gorodetsky, and T. J. Kippenberg, *Phys. Rev. Lett.* **113**, 1 (2014).
- [17] M. Karpov, M. H. Pfeiffer, J. Liu, A. Lukashchuk, and T. J. Kippenberg, *Nat. Commun.* **9**, 1 (2018), [arXiv:1706.06445](https://arxiv.org/abs/1706.06445).
- [18] P. Grelu and N. Akhmediev, *Nat. Photonics* **6**, 84 (2012).
- [19] T. Herr, V. Brasch, J. D. Jost, C. Y. Wang, N. M. Kondratiev, M. L. Gorodetsky, and T. J. Kippenberg, *Nat. Photonics* **8**, 145 (2014).
- [20] S. Wabnitz, *Opt. Lett.* **18**, 601 (1993).
- [21] I. Barashenkov and Y. S. Smirnov, *Phys. Rev. E* **54**, 5707 (1996).
- [22] F. Leo, S. Coen, P. Kockaert, S.-P. Gorza, P. Emplit, and M. Haelterman, *Nat. Photon.* **4**, 471 (2010).
- [23] V. Brasch, M. Geiselmann, T. Herr, G. Lihachev, M. H. P. Pfeiffer, M. L. Gorodetsky, and T. J. Kippenberg, *Science* **351**, 357 (2016).
- [24] M.-G. Suh, Q.-F. Yang, K. Y. Yang, X. Yi, and K. J. Vahala, *Science* **354**, 600 (2016).
- [25] P. Marin-Palomo, J. N. Kemal, M. Karpov, A. Kordts, J. Pfeifle, M. H. Pfeiffer, P. Trocha, S. Wolf, V. Brasch, M. H. Anderson, *et al.*, *Nature* **546**, 274 (2017).
- [26] T. J. Kippenberg, A. L. Gaeta, M. Lipson, and M. L. Gorodetsky, *Science* **361**, eaan8083 (2018).
- [27] B. Shen, L. Chang, J. Liu, H. Wang, Q. F. Yang, C. Xiang, R. N. Wang, J. He, T. Liu, W. Xie, J. Guo, D. Kinghorn, L. Wu, Q. X. Ji, T. J. Kippenberg, K. Vahala, and J. E. Bowers, *Nature* **582**, 365 (2020).
- [28] J. Riemensberger, A. Lukashchuk, M. Karpov, W. Weng, E. Lucas, J. Liu, and T. J. Kippenberg, *Nature* **581**, 164 (2020), [arXiv:1912.11374](https://arxiv.org/abs/1912.11374).
- [29] X. Xue, Y. Xuan, Y. Liu, P.-H. Wang, S. Chen, J. Wang, D. E. Leaird, M. Qi, and A. M. Weiner, *Nat. Photonics* **9**, 594 (2015).
- [30] X. Xue, Y. Xuan, P.-H. Wang, Y. Liu, D. E. Leaird, M. Qi, and A. M. Weiner, *Laser Photonics Rev.* **9**, L23 (2015).
- [31] B. Y. Kim, Y. Okawachi, J. K. Jang, M. Yu, X. Ji, Y. Zhao, C. Joshi, M. Lipson, and A. L. Gaeta, *Opt. Lett.* **44**, 4475 (2019).
- [32] O. B. Helgason, F. R. Arteaga-Sierra, Z. Ye, K. Twayana, P. A. Andrekson, M. Karlsson, J. Schroder, and V. Torres-Company, *arXiv preprint arXiv:2007.02608* (2020).
- [33] M. Karpov, M. H. Pfeiffer, H. Guo, W. Weng, J. Liu, and T. J. Kippenberg, *Nat. Phys.* **15**, 1071 (2019).
- [34] H. Guo, E. Lucas, M. H. Pfeiffer, M. Karpov, M. Anderson, J. Liu, M. Geiselmann, J. D. Jost, and T. J. Kippenberg, *Phys. Rev. X* **7**, 041055 (2017).
- [35] A. Tikan, J. Riemensberger, K. Komagata, S. Hönzl, M. Churaev, C. Skehan, H. Guo, R. N. Wang, J. Liu, P. Seidler, *et al.*, *arXiv preprint arXiv:2005.06470* (2020).
- [36] X. Xue, X. Zheng, and B. Zhou, *Nat. Photonics* **13**, 616 (2019).
- [37] M. H. P. Pfeiffer, J. Liu, A. S. Raja, T. Morais, B. Ghadiani, and T. J. Kippenberg, *Optica* **5**, 884 (2018).
- [38] P. Del’Haye, O. Arcizet, M. L. Gorodetsky, R. Holzwarth, and T. J. Kippenberg, *Nat. Photonics* **3**, 529 (2009).
- [39] J. R. Stone, T. C. Briles, T. E. Drake, D. T. Spencer, D. R. Carlson, S. A. Diddams, and S. B. Papp, *Phys. Rev. Lett.* **121**, 063902 (2018).
- [40] H. Guo, M. Karpov, E. Lucas, A. Kordts, M. H. Pfeiffer, V. Brasch, G. Lihachev, V. E. Lobanov, M. L. Gorodetsky, and T. J. Kippenberg, *Nature Physics* **13**, 94 (2017).
- [41] C. Bao, Y. Xuan, D. E. Leaird, S. Wabnitz, M. Qi, and A. M. Weiner, *Optica* **4**, 1011 (2017).
- [42] H. A. Haus and W. Huang, *Proceedings of the IEEE* **79**, 1505 (1991).
- [43] W. Su, J. Schrieffer, and A. J. Heeger, *Phys. Rev. Lett.* **42**, 1698 (1979).
- [44] D. Dobrykh, A. Yulin, A. Slobozhanyuk, A. Poddubny, and Y. S. Kivshar, *Phys. Rev. Lett.* **121**, 163901 (2018).
- [45] D. Smirnova, D. Leykam, Y. Chong, and Y. Kivshar, *Appl. Phys. Rev.* **7**, 021306 (2020).
- [46] J. K. Asbóth, L. Oroszlány, and A. Pályi, *A short course on topological insulators*, Vol. 919 (Springer, 2016) pp. 997–1000.

# Supplementary Materials: Symmetry protection of topological states in multimode photonic resonator chains

A. Tikan,<sup>1,\*</sup> A. Tushin,<sup>1</sup> J. Riemensberger,<sup>1</sup> M. Churaev,<sup>1</sup>  
K. Komagata,<sup>1,2</sup> X. Ji,<sup>1</sup> R. N. Wang,<sup>1</sup> J. Liu,<sup>1</sup> and T. J. Kippenberg<sup>1,†</sup>

<sup>1</sup>*Institute of Physics, Swiss Federal Institute of Technology Lausanne (EPFL), CH-1015 Lausanne, Switzerland*

<sup>2</sup>*Present address: Laboratoire Temps-Fréquence, Avenue de Bellevaux 51, 2000 Neuchâtel, Switzerland*

## MODE INTERACTIONS IN TWO EVANESCENTLY COUPLED RESONATORS

We examine here the mode interaction of two ring resonators using a perturbation approach. Taking the solution of the Maxwell's equations for single resonator as a basis for the field profile in the coupled system, we derive coupling coefficients between different modes as a function of mode overlaps. The obtained expressions can be used for the exact evaluation of the coupling coefficients for whispering gallery mode resonators, since analytical expressions are known in this case [1, 2], while for integrated microresonator dimers they, however, help to qualitatively understand the mode-crossing mechanism.

We start from the scalar wave equation on electric field in the system comprising two identical evanescently coupled optical resonators. The wave equation

$$\left(\Delta + \frac{n_g^2}{c^2} \frac{\partial^2}{\partial t^2}\right)E = 0 \quad (1)$$

governs the electric field in the media with the group index  $n_g$ . In a single resonator case, rotational symmetry allows one to obtain a set of eigenfrequencies and eigenfunctions supported by the system. Typically there are two polarization mode families (TE and TM), and within each polarization mode family there is a set of eigenfunctions (i.e. states) which have different spatial distributions. In the ideal case, all the eigenfunctions are orthogonal, even if they correspond to degenerate eigenfrequencies. The presence of perturbations which cause the axial symmetry breaking leads to the interaction between the modes breaking, thereby their orthogonality. This interaction manifest itself as avoided mode crossings (AMXs) in the dispersion profile. The AMXs appear at degenerate frequencies, where two different modes have close eigenvalues [3, 4].

The scenario of mode interaction in the photonic dimer is similar to the conventional conventional single resonator case, but the difference arises from the fact that we investigate two sets of eigenmodes which belong to different rings. In order to obtain the coupling coefficients, we employ the perturbation approach. Starting from independent eigenfunctions for both rings, implying at first the infinite distance between the resonators, we decompose the electric field on a series of eigenfunctions and obtain a system of coupled ordinary differential equations on amplitudes of the modes.

We start with a single resonator case which has the group index  $n_{gI}$ . Using the ansatz of harmonic time dependence  $E \rightarrow Ee^{-i\omega t}$ , one obtains the Helmholtz equation

$$(\Delta + n_{gI}^2 k_0^2)E = 0, \quad (2)$$

where  $k_0 = \omega/c$  is the wavenumber. Eq. (2) defines eigenfrequencies  $\omega_\mu^I$  and eigenfunctions  $\Psi_\mu^I$  with orthogonality relation:

$$\int \Psi_\mu^I (\Psi_\nu^I)^* n_{gI}^2 dV = \delta_{\mu,\nu}. \quad (3)$$

Here asterisk stands for complex conjugation. The electric field is  $E = A_\mu^I \Psi_\mu^I$ , where  $A_\mu^I$  is the normalization constant. Note, that same is valid for the second resonator for which it is sufficient simply to replace  $I$  by  $II$ . Moreover, we consider the resonators to be identical, meaning that  $\omega_\nu^I = \omega_\nu^{II}$ .

Now, we suppose that the two resonators are placed closed so their eigenfunctions overlap. In order to exploit the eigenfunctions of each ring, we rewrite the group index  $n_g$  in following form:

$$n_g^2 = \begin{cases} n_{gI}^2 + n_{II} \\ n_{gII}^2 + n_I \end{cases} \quad (4)$$

depending on the basis we want to use. We decompose further the electric field in the following way:

$$E = \sum_i A_i^I(t) \Psi_i^I e^{-i\omega_i t} + \sum_i A_i^{II}(t) \Psi_i^{II} e^{-i\omega_i t}. \quad (5)$$

Substituting this to the Eq. 1 and using the slowly varying envelope approximation ( $d^2 A_i^I/dt^2 \ll \omega_i dA_i^I/dt$ ) we obtain the following equation:

$$\begin{aligned} \Delta E - \frac{n_g^2}{c^2} \frac{\partial^2 E}{\partial t^2} = \\ \sum_i \left( n_{II} \Psi_i^I A_i^I \lambda_i^2 + 2i\lambda_i \dot{A}_i^I \Psi_i^I \frac{(n_{gI}^2 + n_{II})}{c} \right) e^{-i\omega_i t} + \\ \sum_i \left( n_I \Psi_i^{II} A_i^{II} \lambda_i^2 + 2i\lambda_i \dot{A}_i^{II} \Psi_i^{II} \frac{(n_{gII}^2 + n_I)}{c} \right) e^{-i\omega_i t} = 0, \end{aligned} \quad (6)$$

where  $\lambda_i = \omega_i/c$  and  $\dot{A}$  stands for the time derivative of  $A$ . Now, we multiply this equation by  $(\Psi_k^{II})^*$  and integrate it over the whole volume. Using the orthogonality

relation (3), one obtains a system of ordinary differential equations on the mode amplitudes with coupling coefficients proportional to the mode overlap.

Considering the case of two mode families in both resonators, one can derive the matrix model introduced in the main text. In order to keep the same notations, we denote  $A_1^I \equiv a_1$ ,  $A_2^I \equiv b_1$ ,  $A_1^{II} \equiv a_2$ ,  $A_2^{II} \equiv b_2$ . Taking only leading order coefficients, system (6) takes form

$$\begin{cases} \dot{a}_1 &= i(J_{a_1 a_1} a_1 + J_{a_1 a_2} a_2 + J_{a_1 b_1} b_1 + J_{a_1 b_2} b_2) \\ \dot{a}_2 &= i(J_{a_2 a_1} a_1 + J_{a_2 a_2} a_2 + J_{a_2 b_1} b_1 + J_{a_2 b_2} b_2) \\ \dot{b}_1 &= i(J_{b_1 a_1} a_1 + J_{b_1 a_2} a_2 + J_{b_1 b_1} b_1 + J_{b_1 b_2} b_2) \\ \dot{b}_2 &= i(J_{b_2 a_1} a_1 + J_{b_2 a_2} a_2 + J_{b_2 b_1} b_1 + J_{b_2 b_2} b_2), \end{cases} \quad (7)$$

where diagonal terms indicate self-frequency shift due to presence of the coupling sections. They can be expressed through the mode overlap integrals as follows:

$$J_{a_1 a_1} = \frac{\lambda_0 c}{2} \int \Psi_0^I \Psi_0^{I*} n_{II} dV; \quad J_{a_2 a_2} = \frac{\lambda_0 c}{2} \int \Psi_0^{II} \Psi_0^{II*} n_I dV \quad (8)$$

$$J_{b_1 b_1} = \frac{\lambda_1 c}{2} \int \Psi_1^I \Psi_1^{I*} n_{II} dV; \quad J_{b_2 b_2} = \frac{\lambda_1 c}{2} \int \Psi_1^{II} \Psi_1^{II*} n_I dV. \quad (9)$$

Due to the symmetry, the expressions in each line of Eq. (8) are equal. Applying the notations from the main text, we obtain  $\omega_1 = J_{a_1 a_1}$  and  $\omega_2 = J_{b_1 b_1}$ .

The offdiagonal coefficients in system (7) depict the mode interaction. Let us consider the interaction between the fundamental and higher order modes of one resonator. The corresponding coefficients are expressed as

$$J_{a_1 b_1} = \frac{\lambda_1^2 c}{2\lambda_0} \int \Psi_1^I \Psi_0^{I*} n_{II} dV e^{-i(\omega_1 - \omega_0)t}, \quad (10)$$

$$J_{a_2 b_2} = \frac{\lambda_1^2 c}{2\lambda_0} \int \Psi_1^{II} \Psi_0^{II*} n_I dV e^{-i(\omega_1 - \omega_0)t}, \quad (11)$$

$$J_{b_1 a_1} = \frac{\lambda_0^2 c}{2\lambda_1} \int \Psi_0^I \Psi_1^{I*} n_{II} dV e^{-i(\omega_0 - \omega_1)t}, \quad (12)$$

$$J_{b_2 a_2} = \frac{\lambda_0^2 c}{2\lambda_1} \int \Psi_0^{II} \Psi_1^{II*} n_I dV e^{-i(\omega_0 - \omega_1)t}. \quad (13)$$

As one can see, the interaction efficiency is enhanced at the points of degeneracy, where the eigenfrequencies coincide. These points correspond to the exact positions of the mode crossings. In the main text we consider this particular example, thus  $J_{ab}^{\text{int}} = J_{a_1 b_1}|_{\omega_0=\omega_1} = J_{a_2 b_2}|_{\omega_0=\omega_1}$  and  $J_{ba}^{\text{int}} = J_{b_1 a_1}|_{\omega_0=\omega_1} = J_{b_2 a_2}|_{\omega_0=\omega_1}$ , where we assumed the coupling purely real for simplicity.

The coupling coefficients between the fundamental modes of both resonators take form:

$$J_{a_1 a_2} = \frac{\lambda_0 c}{2} \int \Psi_0^{II} \Psi_0^{I*} n_I dV, \quad (14)$$

$$J_{a_2 a_1} = \frac{\lambda_0 c}{2} \int \Psi_0^I \Psi_0^{II*} n_{II} dV, \quad (15)$$

and they are equal due to the symmetry. The corresponding coefficient in the main text  $J_{aa}^{\text{ext}} = J_{a_1 a_2} J_{a_2 a_1}$ . In similar way we express coupling between higher order modes

$$J_{b_1 b_2} = \frac{\lambda_1 c}{2} \int \Psi_1^{II} \Psi_1^{I*} n_I dV, \quad (16)$$

$$J_{b_2 b_1} = \frac{\lambda_1 c}{2} \int \Psi_1^I \Psi_1^{II*} n_{II} dV, \quad (17)$$

with  $J_{bb}^{\text{ext}} = J_{b_1 b_2} = J_{b_2 b_1}$ .

The coefficients governing interactions between fundamental and higher order modes of distinct resonators are placed on the side diagonal of the system (7), and their expressions are by

$$J_{a_1 b_2} = \frac{\lambda_1^2 c}{2\lambda_0} \int \Psi_1^{II} \Psi_0^{I*} n_I dV e^{-i(\omega_1 - \omega_0)t}, \quad (18)$$

$$J_{a_2 b_1} = \frac{\lambda_1^2 c}{2\lambda_0} \int \Psi_1^I \Psi_0^{II*} n_{II} dV e^{-i(\omega_1 - \omega_0)t}, \quad (19)$$

$$J_{b_2 a_1} = \frac{\lambda_0^2 c}{2\lambda_1} \int \Psi_0^I \Psi_1^{II*} n_{II} dV e^{-i(\omega_0 - \omega_1)t}, \quad (20)$$

$$J_{b_1 a_2} = \frac{\lambda_0^2 c}{2\lambda_1} \int \Psi_0^{II} \Psi_1^{I*} n_I dV e^{-i(\omega_0 - \omega_1)t}. \quad (21)$$

As one can see, the interaction increases at degenerate frequencies, and then  $J_{ab}^{\text{ext}} = J_{a_1 b_2}|_{\omega_1=\omega_2} = J_{a_2 b_1}|_{\omega_1=\omega_2}$ ,  $J_{ba}^{\text{ext}} = J_{b_2 a_1}|_{\omega_1=\omega_2} = J_{b_1 a_2}|_{\omega_1=\omega_2}$ . It is important to note, that the intraresonator interaction originates from the mode overlap in the area where both modes decay exponentially (for example see Eq. (10)), when the interresonator coupling originates from the area where one is localized and second one is evanescent (e.g. Eq. (18)). However, it is hard to estimate the ratio between these coefficients because it also depends on the integral along azimuth coordinate. In order to obtain this ration we provide FDTD simulations in Lumerical, which are presented in the next sections.

## MATRIX MODEL

The generalize to the case of N coupled resonators the coupling matrix of the size  $2N \times 2N$  can be represented as follows:

$$i \frac{dU}{dt} = - \begin{pmatrix} -\omega_1 & J_{aa}^{\text{ext}} & & J_{ab}^{\text{int}} & J_{ab}^{\text{ext}} & & \\ J_{aa}^{\text{ext}} & -\omega_1 & \ddots & J_{ab}^{\text{ext}} & J_{ab}^{\text{int}} & \ddots & \\ & \ddots & \ddots & J_{aa}^{\text{ext}} & & \ddots & J_{ab}^{\text{ext}} \\ & & & J_{aa}^{\text{ext}} & -\omega_1 & & J_{ab}^{\text{int}} \\ J_{ba}^{\text{int}} & J_{ba}^{\text{ext}} & & & -\omega_2 & J_{bb}^{\text{ext}} & \\ J_{ba}^{\text{ext}} & J_{ba}^{\text{int}} & \ddots & J_{bb}^{\text{ext}} & -\omega_2 & \ddots & \\ & \ddots & \ddots & J_{ba}^{\text{ext}} & & \ddots & J_{bb}^{\text{ext}} \\ & & & J_{ba}^{\text{ext}} & J_{ba}^{\text{int}} & & J_{bb}^{\text{ext}} \\ & & & & & & J_{bb}^{\text{ext}} & -\omega_2 \end{pmatrix} U, \quad (22)$$

where  $U = (a_1, \dots, a_N, b_1, \dots, b_N)^T$ . The coupling matrix is comprised of four blocks of symmetric tridiagonal matrices implying that empty spaces are zeros. For the calculations presented in the article we suppose that  $J_{ab}^{ext,int}$  and  $J_{ab}^{ext,int}$  are equal due to the apparent symmetry, therefore second and third blocks of the coupling matrix are identical. Blocks one and four are also set to be identical since the difference between  $J_{aa}^{ext}$  and  $J_{bb}^{ext}$  will lead to a simple shift along the direction of the higher-order mode and the mode interaction therefore has to be examined at  $\omega_1 = \omega_2 = 0$ .

## FDTD SIMULATIONS OF THE COUPLING SECTION

In order to confirm the coupling coefficient ratio expected from the analytical model of four-mode interaction, we provide FDTD simulations (*Lumerical FDTD Solutions*) of the coupling section of the photonic dimer. We constructed a model of a dimer device comprised of two 200 GHz ring resonators. The silicon nitride ( $\text{Si}_3\text{N}_4$ ) resonator core is fully cladded with Silicon dioxide ( $\text{SiO}_2$ ). Both resonators are  $1.5 \mu\text{m}$  wide and  $0.82 \mu\text{m}$  high, with sidewall angle  $\alpha = 90^\circ$ , as used in the experiments. The mode source was configured to inject at an angle of  $20^\circ$  with unity power, as shown in Fig. 1a, and to excite only the fundamental mode of the ring. In this way, we shrank the simulation region to  $100 \times 30 \times 8 \mu\text{m}^3$  and the simulation time to 900 fs, which is sufficient to capture correctly the coupling to higher-order modes with much less processing time. The boundary of the simulation region is fixed with a perfectly matched layer (PML) condition to absorb the incident light and therefore to prevent backreflection. The light field then propagated in the full simulation region until a stationary

state is reached. Monitors M0, M1 and M2 recorded the spatial distributions of the mode source, the transmitted field and the coupled field respectively. In addition, two mode expansion monitors were placed in the same plane as M1 and M2 to calculate the power of selected resonator eigenmode ( $\text{TE}_{10}$ ). All powers are normalized as they derived from the resonator fundamental mode that is launched with unity power. The coupling coefficients,  $J_{ab}^{int}$  and  $J_{ab}^{ext}$ , are estimated using a simplified coupled mode equation, by  $J_{ab}^i = D_1 \times \arccos(\sqrt{1 - P_{ab}^i})$ , where  $D_1/2\pi = FSR$ .

Numerical simulations reveal that increasing the gap distance between two resonators,  $J_{ab}^{ext}$  rapidly (eventually exponentially) decays, while  $J_{ab}^{int}$  remains constant at 18 GHz except the region  $0.2\text{-}0.4 \mu\text{m}$  where it demonstrates lower values at mesh order 3 as shown in Fig. 1. Careful analysis of the ratio  $J_{ab}^{int}/J_{ab}^{ext}$  convergence with increasing mesh order (decreasing the simulation net size) suggests that the ratio converges to unity. The simulations with mesh order 3 gives a considerable error of  $\approx 35\%$ .

The coupling of the ring resonator to the bus and drop waveguides was also simulated at  $0.3 \mu\text{m}$ , rendering a converged result of 0.75 GHz, which contributes to the coefficient  $J_{ab}^{int}$ .

---

\* [alexey.tikan@epfl.ch](mailto:alexey.tikan@epfl.ch)

† [tobias.kippenberg@epfl.ch](mailto:tobias.kippenberg@epfl.ch)

- [1] M. L. Gorodetsky and A. E. Fomin, *IEEE Journal of Selected Topics in Quantum Electronics* **12**, 33 (2006).
- [2] B. Sturman, E. Podivilov, C. S. Werner, and I. Breunig, *Phys. Rev. A* **99**, 013810 (2019).
- [3] J. Zhu, S. K. Ozdemir, Y.-F. Xiao, L. Li, L. He, D.-R. Chen, and L. Yang, *Nat. Photon.* **4**, 46 (2010).
- [4] D. V. Strekalov, C. Marquardt, A. B. Matsko, H. G. L. Schwefel, and G. Leuchs, *Journal of Optics* **18**, 123002 (2016).

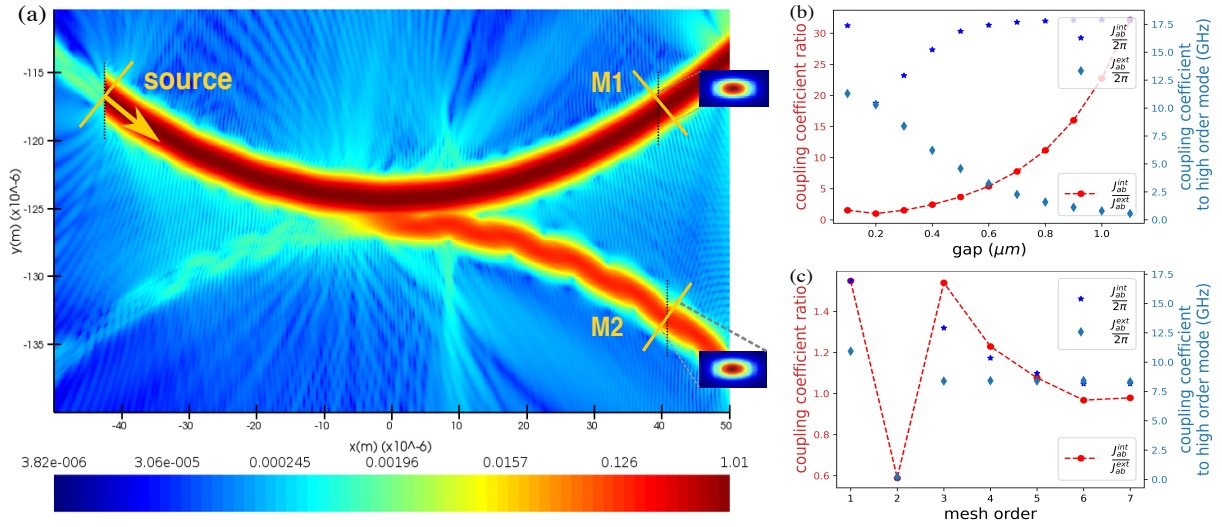


FIG. 1. FDTD simulations of the coupling section. (a) Normalized electric field distribution shown in log scale, the colour bar measures the field power. The mode source is launched normal to the waveguide propagation direction with unity power. Insets present spatial field distributions recorded by monitor M1 and M2. The gap distance is set as  $0.3 \mu m$ . (b) Dependence of the coupling coefficients to higher-order modes on gap distance, at mesh 3. (c) Convergence of the coupling coefficients to higher-order modes with mesh order, as illustrated by the red dashed line, the coupling coefficient ratio converges closely to unity.